Ethylbenzene Diffusion in Polystyrene: United Atom Atomistic/ Coarse Grained Simulations and Experiments

V. A. Harmandaris, N. P. Adhikari, N. F. A. van der Vegt, and K. Kremer*

Max-Planck-Institut für Polymerforschung, D-55128 Mainz, Germany

B. A. Mann,† R. Voelkel, H. Weiss, and CheeChin Liew

Polymer Research, BASF Aktiengesellschaft, D-67056, Ludwigshafen, Germany

Received January 24, 2007; Revised Manuscript Received July 4, 2007

ABSTRACT: A detailed study of the structure and the dynamics of the polystyrene− (PS−) ethylbenzene (EB) polymer−penetrant system is presented. The work combines dual scale (atomistic/coarse grained) simulations and experiments. United atom atomistic *NPT* molecular dynamics simulations as well as coarse-grained (CG) molecular dynamics simulations have been executed and the ability of the CG simulations to predict the dynamic properties of the polymer/penetrant system is examined. The results are directly compared to pulse-field gradient nuclear magnetic resonance measurements. The coarse-grained simulations, which are much faster than atomistic ones, are capable of describing the diffusion of EB molecules. This opens up the way to study polymer/penetrant systems difficult to reach by experiment but of technological importance.

1. Introduction

The accurate knowledge of the transport properties of polymeric liquids is extremely important for technological applications, since these properties govern their processability in the molten state as well as final product properties. Efforts to predict these properties through either theoretical arguments or detailed computer simulation studies have attracted considerable interest in the literature over many years.[1−6] In addition to predicting the diffusion properties of pure polymer melts, the diffusivity of small dissolved molecules is of equal importance. The average molecular weight and its distribution, for example, are among the physical properties influenced by the diffusion-controlled termination step of free radical polymerization reactions. In addition molecular transport of small molecules affects the mixing of plasticizers with polymers, the removal of residual monomer or solvent from polymers through the devolatilization process, and the formation of films, coatings, and foams from polymer−solvent mixtures.[1]

From the theoretical point of view, a classical theory for describing the diffusion of small molecules in polymer−penetrant systems is the free volume theory.[7] This theory is based on the assumption of Cohen and Turnbull[8] that molecular transport relies on a continuous redistribution of free volume elements within the liquid.[9] The availability of free volume within the system controls the molecular transport. More recently, building on the ideas of the free volume theory, von Meerwall et al.[10,11] proposed a combined theory for the diffusion of binary systems, based on the notions of the monomeric friction coefficient, intrinsic thermal activation and host free volume effects, with particular attention to the chain-end contribution.

Experimentally the diffusion of small molecules in polymer systems has been studied with various techniques.[12,13] For example, Wagoner et al.,[12] using nuclear magnetic resonance (NMR), measured the self-diffusion coefficients of several solvents in different polymers and compared their results with the predictions of the free volume theory.

† Deceased.

Atomistic molecular dynamics (MD) simulations are powerful tools for predicting the dynamics of molecular systems. Therefore, it has been used quite often in the literature for studying penetrant dynamics in polymer/penetrant systems.[14−28] For example, the diffusion of small gaseous penetrants in a polymer matrix was found to take place via a hopping process,[15,17] whereas the diffusion of phenol molecules in bisphenol A-polycarbonate melt revealed a transition from hopping toward more continuous diffusion at high temperatures.[24] In addition to equilibrium MD, nonequilibrium MD methods have been also applied, for example, to calculate tracer diffusivities in *n*-alkane liquids and polymers.[23] More recently the diffusion of binary blends on *n*-alkanes and polymers has been studied. The results obtained for the solvent self-diffusion coefficient at low solvent concentrations are in good agreement with the free volume theory.[25,26]

Despite the quite large number of simulation efforts, usually only polymeric systems with relatively low molecular weight are modeled in atomistic detail and even then only the diffusion of the penetrant can be studied. The reason for this should be sought in the difficulties associated with the simulation of polymeric systems resulting from the wide spectrum of time and length scales characterizing their dynamics and structure. To overcome these difficulties, coarse grained (CG) dynamic simulations can be used. To this purpose various coarse-grained models have been used for the study of the dynamics of bulk polymers (see, for example, refs 2, 4, and 29−34).

Here we present a hierarchical simulation methodology that combines microscopic (atomistic) and mesoscopic (CG) modeling and that is used for the study of the molecular transport in polymer−penetrant systems. Key features of our approach are as follows: (a) the execution of atomistic simulations of some reference systems, which in our case is a united-atom model;[35] (b) the extension of a CG model, developed recently,[34] to study binary mixtures; (c) a detailed "time mapping" of the dynamics in the CG description using the data obtained from the atomistic simulations. The whole approach is applied to a typical polymer/penetrant system, which is relevant in polymer processing, i.e., binary blends of atactic polystyrene (PS) and ethylbenzene (EB).

10.1021/ma070201o CCC: $37.00
Published on Web 08/21/2007

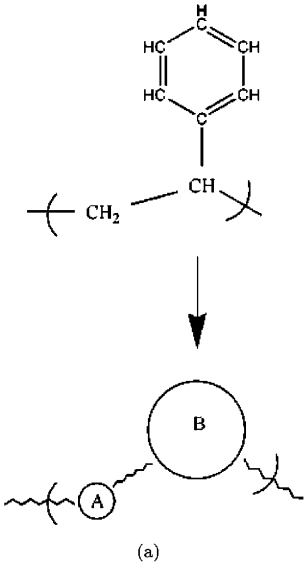

(a)

Figure 1. Atomistic and coarse-graining representation of a PS monomer.

Additionally, pulse-field gradient nuclear magnetic resonance (PFG NMR) experiments have been performed and the simulation findings are compared to the experimental data. The goal of the present work is twofold. The first is to present a detailed study of the diffusivity of a penetrant (EB) in polymer/penetrant (PS/EB) mixtures through PFG NMR experiments and simulation techniques. Second is to examine the ability of simulation methodologies, and mainly CG techniques, to predict dynamical properties of polymer−penetrant mixtures. The latter addresses the question, whether CG simulations, which have been proven to properly model polymer dynamics[30,31,36] (for a general overview, see ref 32), can be extended to the dynamics of low molecular weight additives. In this work, we will present results on the dynamics of EB in PS/EB systems using a CG description that is relatively close to the chemistry of the real system. Using information from short atomistic runs, it is shown that the molecular transport of the penetrant in the polymer matrix can be described quantitatively through CG models.

The remainder of the manuscript is organized as follows. Section 2 presents the hierarchical modeling approach describing the atomistic and the CG simulations of EB and PS systems. Section 3 describes in details the experiments performed in this work. Results from the simulations and the experiments for the structural and dynamical properties of these systems are presented in section 4. Finally, our findings and conclusions are summarized in section 5.

2. Hierarchical Modeling

2.1. Atomistic Simulations. For the atomistic modeling of the PS/EB systems we choose the TraPPE united atom (UA) model,[35] which reproduces the density of PS over a range of temperatures.

In the united atom description of this model each PS monomer is described with eight united atom groups (see Figure 1). Five different types of united atoms (CH_3, CH_2, CH, C_{aro}, and CH_{aro}) are defined in a PS chain, whose nonbonded interactions are described by pairwise-additive Lennard-Jones potentials. All bond lengths were kept rigid whereas a harmonic potential is used to describe bond angle bending. Standard torsional potentials are used to describe rotations along bonds in the aliphatic backbone. Finally, improper dihedral potentials are used to keep the phenyl ring planar as well as to maintain the tetrahedral configuration around the sp3 hybridized carbon connecting the phenyl ring. More details about the atomistic force field can be found elsewhere.[34,35]

The molecular dynamics package GROMACS[37] was used to perform all the atomistic MD simulations reported in the present study. Various PS/EB systems have been simulated. The molecular weight of the PS in all systems is 10 kDa (10000 g/mol) whereas the temperature range is from 398 to 473 K and the EB concentration varies from 1% to 10% per weight. PS chains are atactic. All PS/EB mixtures that have been simulated are presented in Table 1a.

The setup of the initial configurations was performed in several stages. First, at a very low density of about 0.0008 g/cm^3, well separated chains and the added EB molecules were equilibrated at a high temperature of $T = 600$ K, ensuring the full relaxation of the system without any overlap. Subsequently a very long isothermal−isobaric, *NPT*, run at $T = 463$ K was performed. The melt radial distribution functions for the lowest EB content, the case, where equilibration is most difficult and time-consuming, have been checked in comparison to melts obtained in a different study.[34] The obtained radial distribution functions showed structure up to a distance of about 20 Å and have been shown to excellently agree to experiment. The data of the present study perfectly coincide with these results. Thus, the polymeric matrix is well equilibrated on scales relevant for the purpose of the present investigation.[49] All *NPT* MD production runs have been conducted at $P = 1$ atm using the Berendsen thermostat (coupling time 0.1 ps) and barostat (coupling time 2.0 ps).[38] Initial configurations for other temperatures were obtained by cooling or heating via long *NPT* MD runs. This cooling (or heating) step could be problematic if the polymer chain dimensions change significantly through the two temperatures because the MD runs will not be long enough to fully equilibrate the system. In the range of temperatures studied here, this is not a problem as PS end-to-end distances change less than 5% (for PS $d(\ln C_\infty)/dT = -0.9 \times 10^{-3}$ [39]).

Nonbonded interactions were cut off beyond 1.4 nm. Tail corrections for the energy and pressure were applied.[37] The integration time step was 2 *fs* whereas the overall simulation time of the production runs ranged from 20 to 100 ns depending on the molecular weights of the systems studied. We should also note here that for computational reasons rather small PS/EB systems have been studied based on the TraPPE force field model. Therefore, despite the very long atomistic simulations, data for the asymptotic diffusion coefficient of EB at low EB concentration ($w_{EB} = 0.01$) are statistically unreliable, due to the small number of EB molecules (only 8) present in these systems. For this reason these atomistic runs, as well as those for the systems at the lower temperature ($T = 398$ K), were used only for the calculation of the density.

2.2. Coarse Grained Simulations. The CG dynamic simulations of the polymer−penetrant systems have been performed using a previously developed CG model for PS[34] and an accordingly adjusted coarse grained EB model. In this CG model one monomer of a PS chain is mapped on two effective coarse grained beads (see Figure 1), i.e. the coarse-graining scheme is a 2:1 model. The CH_2 group of the backbone chain represents one coarse-grained effective bead (type "A"), which in this case coincides with one united atom of our atomistic reference model, whereas the remaining CH group of the monomer in the backbone together with the phenyl ring is mapped to another effective coarse-grained bead (type "B"). This mapping scheme was chosen because of mainly two advantages, namely; not

Table 1. PS/EB Systems Simulated in This Work and Experimental Samples

(a) Simulated

method	no. of PS mers	T(K)	w_{EB}	no. of PS (EB) molecules
atomistic MD	96	398, 423, 448, 463	0.1, 0.05, 0.01	9 (96), 9 (46), 9 (8)
CG MD	96	398, 423, 448, 463	0.1, 0.05, 0.01	50 (533), 50 (253), 50 (48)

(b) Experimental

PS M_w	PS M_w/M_n	T (K)	w_{EB}
10 (kDa)	1.07	383, 398, 423, 433, 448, 463, 473	0.1, 0.05, 0.01

Table 2. Densities of PS/EB Systems Obtained from Atomistic *NPT* MD Simulations.

w_{EB}	T (K)	ρ (g/cm^3)
0.01	398	1.030 ± 0.005
	423	1.020 ± 0.005
	448	1.008 ± 0.005
	463	0.998 ± 0.005
0.05	398	1.020 ± 0.005
	423	1.007 ± 0.005
	448	0.995 ± 0.005
	463	0.985 ± 0.005
0.1	398	1.008 ± 0.005
	423	0.993 ± 0.005
	448	0.980 ± 0.005
	463	0.975 ± 0.005

loosing too much structural details in comparison to the all-atom system and to be fast enough in order to be used for the study of the long time dynamics of polymer melts. At the same time, for the present mapping scheme, it is relatively easy to reinsert all the atomistic details into the CG configurations.[34] Furthermore, chain tacticity is captured in our CG model through the use of bond angle and dihedral potentials that depend on the dyad sequence along the chain. Structure on both the monomeric-segmental level (distribution of dihedral angles) as well as on the level of the whole chain (internal distances, radius of gyration) are found in good agreement with that predicted by long atomistic runs and with experimental data.[34] In the CG description of the EB penetrant, the EB molecule is described with two (one "A" and one "B") CG beads. The parameters for these two beads (size, mass, interaction potential) correspond to those of the "A" and "B" beads of a PS monomer respectively. Finally, we note that with the methodology used in the present CG model unphysical chain-crossing is directly avoided. More details about the CG force field and the validation of the CG model in structural and dynamical properties of bulk PS can be found elsewhere.[34]

All coarse-grained MD simulations have been performed in dimensionless LJ units using m_A to scale all masses, $\sigma_{AV} = (\sigma_A + \sigma_B)/2 = 4.25$ Å to scale all lengths and $\epsilon = kT$ to scale all energies. By doing this a suitable unit of time τ can be defined as $\tau = \sqrt{m_A {\sigma_{AV}}^2/\epsilon}$. Note however that, even though τ has the unit of time, it is the physical time only up to a model specific prefactor. The CG systems studied are presented in Table 1a. All the CG runs have been conducted under *NVT* conditions at the density obtained from the atomistic *NPT* simulations (see Table 2). To keep the temperature constant a Langevin thermostat is used, with friction coefficient $\Gamma = 1.0\ \tau^{-1}$. Such a thermostat can be applied as long the friction resulting from the molecular interaction is significantly higher and no long range hydrodynamics effects play a role. Both apply to the present study.[2,36,40,41] The dynamical efficiency of the mesoscopic simulation (around 3 orders of magnitude compared to the atomistic runs[34,44]) allows us to simulate much larger systems for longer times, resulting in more accurate results for the dynamic properties. This is particularly important for the systems with the lower concentration of EB ($w_{EB} = 0.01$), for which penetrant diffusivities can be accurately calculated, in contrast with the small systems studied in full atomistic detail. Finally we should also note that in principle different bonded CG potentials should be used for each temperature.[34] However, for the range of temperatures studied here, the differences between CG potentials are indistinguishable. Thus, in all CG simulation in this work the bonded CG potentials determined at a reference temperature ($T = 463$ K) were used. An additional point has to do with the ability of the CG model to reproduce the temperature dependence of the structural properties, such as the equilibrium end-to-end distance, $\langle R^2 \rangle$. In the present CG simulations, even if it is difficult to calculate accurately $\langle R^2 \rangle$ because of the small number of polymer chains, we observe that $\langle R^2 \rangle$ decreases around 4−4.5% as the temperature increases from 398 to 463 K. Within the error this is in good agreement with the experimental dependence of the characteristic ratio (for PS $\mathrm{d}(\ln C_\infty)\mathrm{d}T = -0.9 \times 10^{-3}$ [39]), which decreases around 5.5% in the same temperature range. Finally all CG MD simulations of the PS/EB systems have been performed using the ESPResSO package.[42]

3. Experiments

3.1. Pulsed-Field-Gradient NMR. Pulsed field gradient NMR measurements of the diffusion coefficient of ethylbenzene inside a polystyrene matrix were run on a Bruker Avance 400 NMR spectrometer, equipped with a 9.4 T wide bore magnet and Bruker diffusion accessory. A self-shielded gradient coil (type Diff60) mounted onto a micro5 body allows for gradients up to 24 T/m followed by spectroscopic detection. The ^{1}H high temperature insert can be operated at temperatures up to 473 K. Temperature was checked with a dummy sample containing a thermocouple and always was within less than ±1 K of the nominal value.

A typical stimulated echo diffusion experiment involved 16 equidistant steps in gradient strength, covering the range of 0.05−23 T/m at low temperature (383 K) and 0.05−2.5 T/m at high-temperature (473 K) to ensure full attenuation of the EB signal at the highest gradient strength, with the other parameters set as follows: duration of the gradient $\delta = 1$ ms, time of diffusion $\Delta = 20$ ms, 16 accumulations each, waiting time 2 s. Spectroscopic detection is essential to distinguish the weak signal of only 1% EB. A typical ^{1}H NMR spectra for a PS/EB system ($w_{EB} = 1\%$, $T = 463$ K) is shown in Figure 2. A rather long echo time, such as $t_{NMR} = 10$ ms, proves advantageous. It completely suppresses the PS signal at low temperatures and keeps the PS signal low up to about 448 K (for example, less than 50% of the signal intensity in the aliphatic region is from PS at 438 K in the 5% sample, i.e., the PS signal is suppressed by a factor of about 10 by exploiting T_2 effects). Indeed, at high-temperature (≥448 K) and high concentration of EB (10% sample) T_2 of PS gets longer and starts to hamper precision of the diffusion measurement unless τ is further increased. During data evaluation it proves sufficient to take account of the PS "background" signal by including a constant offset into the semilog fit of the data, as the PS signal is not attenuated by the gradients used here, the diffusion of PS being 3 orders of magnitude slower. Diffusion constants of EB, D_{EB}, are plotted vs $1/T$ in Figure 7 and shown in Table 3. The error bar is around 5%.

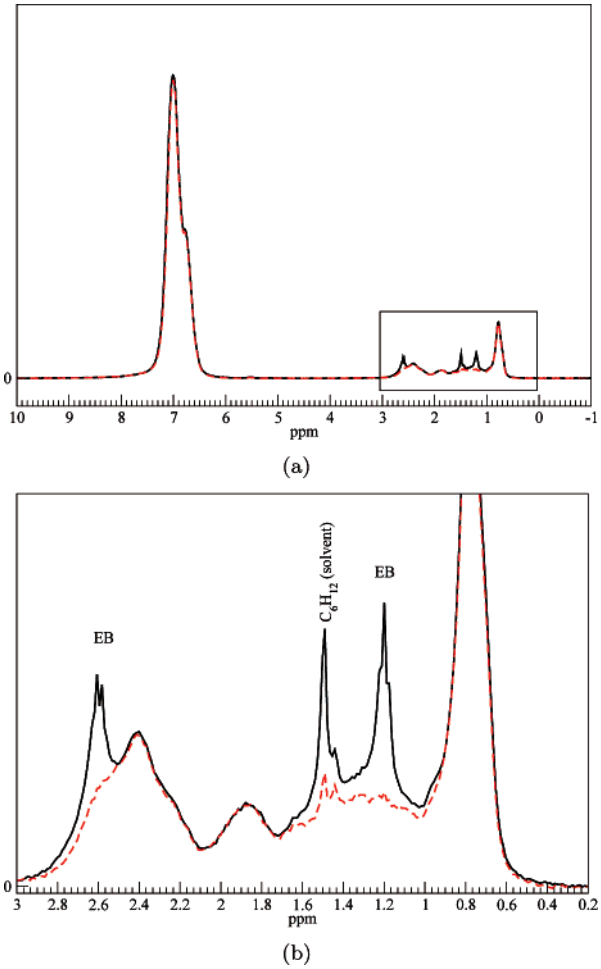

Figure 2. ^{1}H NMR spectra obtained in an PFG experiment on PS (MW = 10kDa) + 1%EB. A full EB spectrum (gradient 0.05 *T*/m only, full line) and a spectrum with a gradient (5 *T*/m, dash line) fully attenuating the EB signal but not the PS is shown ($T = 463$ K, $\Delta = 20$ ms, $\delta = 1$ ms, $\tau = 15$ ms, 32 scans). The PS signal is deliberately scaled down by choosing a long echo time τ. Key: (a) full spectra; (b) EB signal.

Table 3. Diffusion Coefficient of EB, D_{EB}, Obtained from PFG NMR Experiments and Simulations. D_{EB} from CG Simulations before and after the Time Mapping Is Shown.

w_{EB}	T (K)	D_{EB}^{EXP} (10^{-3} Å^2/ps)	D_{EB}^{AT} (10^{-3} Å^2/ps)	D_{EB}^{CG} (Å^2/τ)	D_{EB}^{CG} (10^{-3} Å^2/ps)
0.01	398			0.40 ± 0.01	1.17 ± 0.5
	423	0.78 ± 0.04		0.49 ± 0.01	3.5 ± 1.1
	433	1.50 ± 0.07			
	448	3.70 ± 0.15		0.53 ± 0.01	13.0 ± 2.2
	463	7.90 ± 0.4		0.56 ± 0.02	29.5 ± 3.0
	473	17.0 ± 0.8			
0.05	398	0.86 ± 0.05		0.49 ± 0.01	8.9 ± 1.0
	423	4.50 ± 0.2	20.0 ± 2.0	0.565 ± 0.02	21.0 ± 1.5
	433	7.50 ± 0.4			
	448	12.8 ± 0.6	43.0 ± 3.0	0.63 ± 0.02	42.5 ± 2.5
	463	23.9 ± 1.1	54.0 ± 3.0	0.65 ± 0.02	54.0 ± 3.0
	473	31.4 ± 1.6			
0.1	398	1.50 ± 0.07		0.56 ± 0.02	28.0 ± 2.0
	423	6.80 ± 0.4	48.0 ± 3.0	0.63 ± 0.02	47.5 ± 2.0
	433	10.7 ± 0.5			
	448	19.9 ± 0.9	75.0 ± 3.0	0.71 ± 0.02	74.0 ± 2.5
	463	33.0 ± 1.7	99.0 ± 4.0	0.73 ± 0.03	98.5 ± 3.0
	473	49.0 ± 2.5			

3.2. Materials. Special care was taken in sample preparation to ensure correct and equal concentration of EB anywhere in the sample: The NMR tube of 5 mm O.D. is filled with an appropriate amount of EB, then PS powder from anionic polymerization (molecular weight 10 000 g/mol, $M_w/M_n = 1.07$) is added while controlling the weight until the desired ratio of EB vs PS is reached. Typically around 200 mg of PS are used to obtain a filling height of about 2.5 cm after compaction of the powder. A tightly fitting glass rod is put on top of the sample after flushing with nitrogen, finally sealing the tube. It proved necessary to keep the sample at 423 K (150 °C) for 65 h to ensure homogeneity of EB within the sample, checking homogeneity by magnetic resonance imaging. Filling height after annealing is about half that of the powder and restricts the sample to the area where the gradient applied is linear. The gas volume in the final sample is less or at maximum the same as that of the polymer plug. It is important to avoid any large empty space above the sample and especially outside the heated zone. Major evaporation and condensation of EB in the cold upper zone of the tube and thus loss of EB from the polymer plug is prevented by putting a tight glass rod on top of the sample.

Polystyrene samples of roughly 10 kDa where synthesized by means of anionic polymerization and thus being atactic. The samples were almost monodispersive ($M_w/M_n = 1.07$) and the molecular weight distribution has been controlled by means of size exclusion chromatography.

3.3. Characterization Techniques. Size exclusion chromatography (SEC) experiments were carried out with a modular instrument consisting of a Waters model 510 pump, a sample injector, a Waters 410 differential refractometer, and a UV detector Spectra Series UV 100. The stationary phase was 5 styrene−divinylbenzene gel columns "PSS SDV linear M" (300 × 8 mm each; particle size 5 μm) of Polymer Standards Service GmbH, Mainz, Germany (temperature kept at 308 K). THF was the carrier solvent with a flow rate of 1.2 mL/min. The Instrument was calibrated with PS standards (MG 500−5 000 000 g/mol, PS calibration kit of Polymer Laboratories, England). Sample injection was 160 μL, with concentration 2 mg/mL. Detection was carried out by monitoring RI (refractive index) and UV (at 254 nm). Data processing was done with WinGPC 6.20 (Polymer Standards Service GmbH, Mainz, Germany)

4. Results

4.1. Density and Structure. First the density and the structural properties of the simulated binary systems and the dependence of these properties on the concentration of the penetrant component w_{EB} are checked.

Densities of the EB/PS mixtures, obtained from the atomistic *NPT* MD simulations are shown in Table 2. As expected an increase of the EB concentration leads to a small decrease of the overall density. Neither polymer dimensions (mean square chain end-to-end distance and mean square radius of gyration) nor local conformations (dihedral angle distributions) were affected in a detectable way by the penetrant in the range of concentrations studied here.

Direct information about structural features of the polymer/penetrant systems can be obtained by inspecting the intermolecular pair distribution functions $g(r)$. The $g(r)$'s obtained from the atomistic simulations are shown in Figure 3. In these graphs correlations between *all* united atom groups belonging to different molecules are taken into account. The $g(r)$'s for the PS−PS, EB−EB and EB−PS pairs for two different systems ($w_{EB} = 0.1$, $T = 463$ K and $w_{EB} = 0.01$, $T = 463$ K) are given. The intermolecular $g(r)$ for the PS−PS pair displays less structure than for the PS−EB and the EB−EB pairs and approaches 1 only after 15−20 Å. On the other hand $g(r)$ of the PS−EB pair shows a much different structure with a peak appearing at around 6 Å. Concerning the dependence of the curves on the concentration of EB, $g(r)_{PS-PS}$ decreases as the concentration of EB increases. In agreement with that, $g(r)$ for the PS−EB pairs, $g(r)_{PS-EB}$, slightly increases as w_{EB} increases. The same is observed for the EB−EB case, $g(r)_{EB-EB}$, for which an increase in w_{EB} seems to increase the $g(r)_{EB-EB}$. However

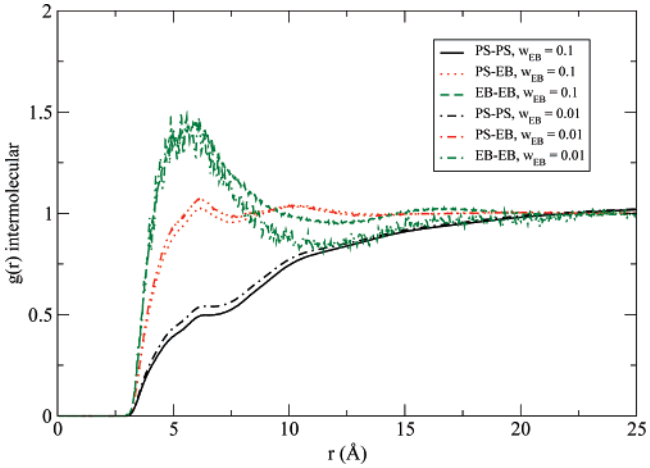

Figure 3. Intermolecular atom−atom distribution function for two PS/EB system ($w_{EB} = 0.1$, $T = 463$ K and $w_{EB} = 0.01$, $T = 463$ K) obtained from atomistic MD simulations.

this tendency is very small and due to low statistical accuracy of the simulations at the low EB concentrations (for $w_{EB} = 0.01$ only 8 EB molecules are present) specific conclusions about the PS−EB, as well as the EB−EB, correlations cannot be obtained. Finally, the intermolecular pair distribution function for the other temperatures display the same behavior.

Another interesting aspect is the comparison of the CG simulations with the atomistic ones at the level of the local structure. To do this we analyze the intermolecular distribution functions of the monomer center of mass for both CG and atomistic simulations of a specific PS/EB system. Parts a−c of Figure 4 show the intermolecular monomer center of mass pair distribution functions, $g(r)^{mon}$, for the PS−PS, PS−EB and EB−EB monomer center-of-mass pairs in a PS/EB mixture ($w_{EB} = 0.1$, $T = 463$ K) obtained from the atomistic runs (full lines) and from the CG simulations (dashed lines). As we can see from Figure 4a there are, as expected, differences between the atomistic and the CG $g(r)$ for the PS−PS center of mass pairs at small distances. The $g(r)^{mon}_{PS-PS}$ calculated from the atomistic runs is more structured compared to the one obtained from the CG simulations. The peaks at 6 and 11 Å correspond mainly to phenyl−phenyl correlations[34] and are smeared out in the CG representation due to the use of spherical beads as well as the use of repulsive bead−bead interactions. Note that if the structure is instead analyzed in terms of CG bead−bead correlations, then the agreement between the atomistic and the CG simulations are better. Similar observations hold for the PS−EB pairs where again a more structured $g(r)^{mon}_{PS-EB}$ is obtained from the atomistic runs. Concerning the EB−EB center-of-mass correlations, $g(r)^{mon}_{EB-EB}$, the matching between the atomistic and the CG simulations, shown in Figure 4c, is remarkable. This is particular important for this work, since we are more interested in the dynamics of EB. In addition, this EB−EB radial distribution function is identical to $g(r)^{mon}_{EB-EB}$ obtained from atomistic simulations of an ethylbenzene gas at the same number density and temperature (not shown), indicating no or only very weak specific correlations due to the polymer matrix. In Figure 5 snapshots of the EB molecules for the PS/EB system with $w_{EB} = 0.1$ and $T = 463$ K obtained from the atomistic (a) and the coarse grained (b) simulations are shown (only the EB and not the polymer molecules are shown). As we can see the clustering of EB molecules is very weak. We here are mostly interest in the diffusion of the EB monomers. This means that at the length (or time) scales where the structural correlations between the CG (EB and polymer) center of mass differ from

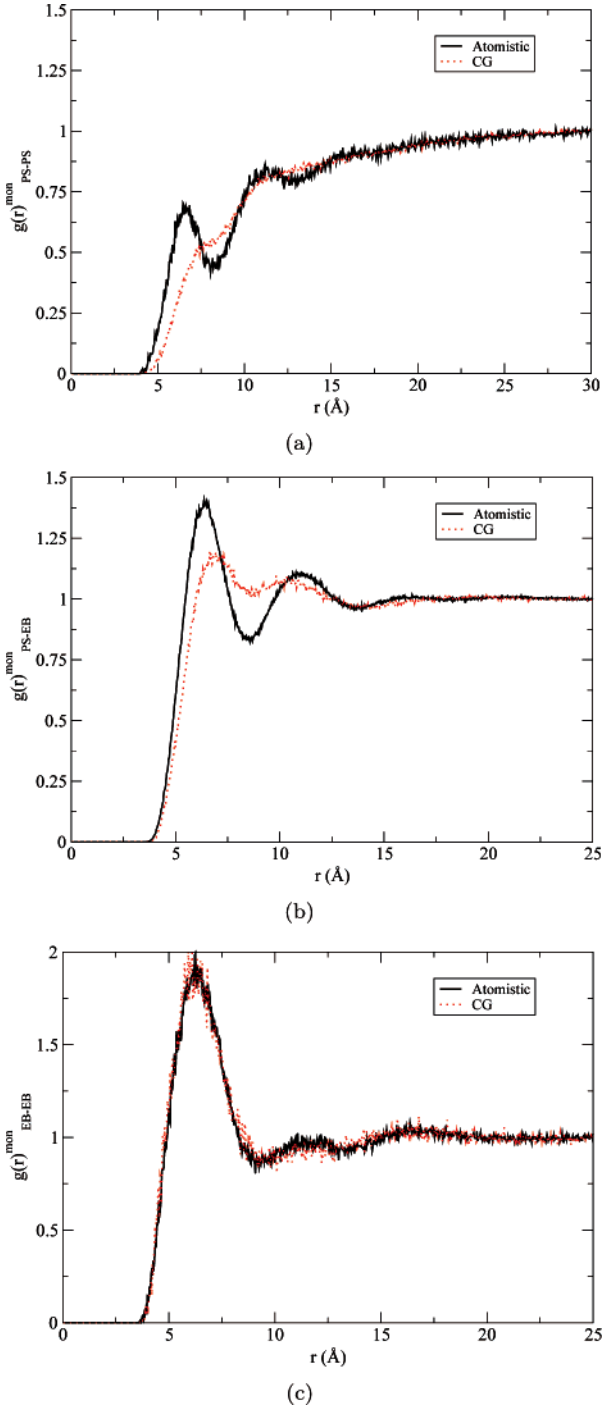

Figure 4. Intermolecular monomer center of mass pair distribution functions obtained from atomistic and CG simulations for a specific PS/EB system ($w_{EB} = 0.1$, $T = 463$ K): (a) PS−PS; (b) PS−EB; (c) EB−EB.

the atomistic one we also expect analogous deviations for the dynamics. For this reason, we have chosen to perform the structural analysis on the level of the EB monomers' center of mass for both the atomistic and CG simulations. The analogous analysis on the level of the "A" and "B" CG beads gives no additional information for this work.

4.2. Dynamics of EB. It is the purpose of the present work, to investigate the possibilities to study the diffusion of small scale additives in specific polymeric melts by coarse graining computer simulations. This is not straightforward at all, as even the very moderate coarse graining steps employed here already apply to the characteristic scales of the additives. To do this

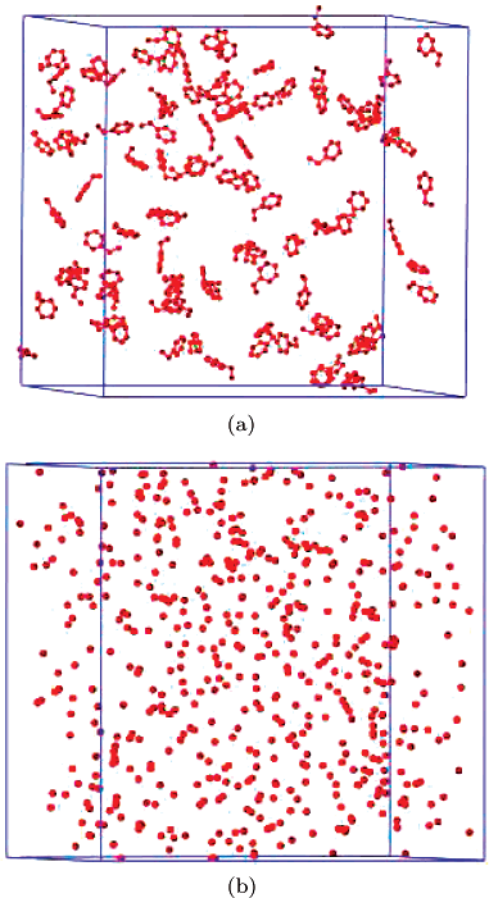

Figure 5. Snapshot of EB molecules in a PS/EB matrix for a PS/EB system ($w_{EB} = 0.1$, $T = 463$ K) obtained from atomistic (a) and coarse grained (b) MD simulations.

we analyze our data in three steps. We first compare the results from the atomistic united atom simulations to NMR experiments. The employed UA model is the basis for the coarse graining procedure, as explained before. Since however this model itself contains a very first coarse graining step by simulating CH and CH_2 superatoms, a careful comparison to experiment is even more needed as it would be anyhow also for all atom simulations. Then the CG simulations are analyzed and compared to the atomistic simulation data. In a third step, both are then again related to each other and to experiment. At a first glance such a procedure might look complicated. As we will however show, the temperature dependence of the results and the time mapping between the different simulations can be rationalized that way, leading to a rather efficient method to study the diffusion of additives by CG simulations.

4.2.1. Dynamics of EB: Atomistic (UA) vs NMR Experiment. The self-diffusion coefficient D_i of component i ($i = 1$, 2) in the binary polymer/penetrant systems is calculated from the linear part of the mean-square displacement (MSDs) of the center of mass of component i, $\langle (R^i_{cm}(t) - R^i_{cm}(0))^2 \rangle$, as a function of time using the Einstein relation:

$$D_i = \lim_{t \to \infty} \frac{\langle (R^i_{cm}(t) - R^i_{cm}(0))^2 \rangle}{6t} \qquad (1)$$

Parts a and b of Figure 6 show plots of the time dependent diffusion coefficient of the EB component, as a function of inverse time, $1/t$, for two typical PS/EB systems ($w_{EB} = 0.1$ at $T = 463$ K and $T = 448$ K) taken from the (a) atomistic MD simulations and (b) CG MD simulations. From the long-time

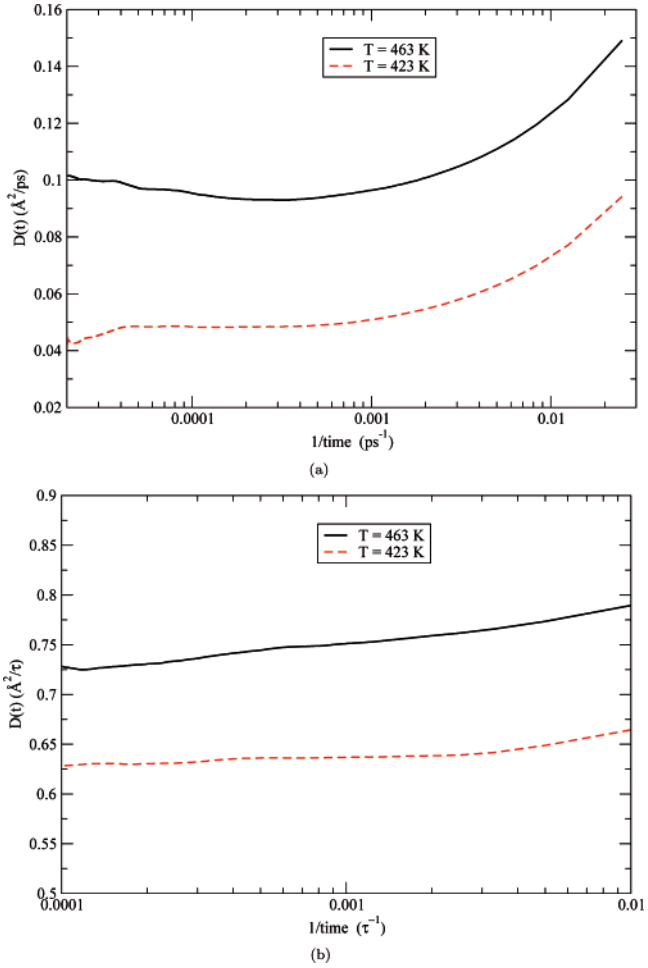

Figure 6. Time dependent diffusion coefficient of EB for two systems with $w_{EB} = 0.1$. from (a) atomistic and (b) CG simulations.

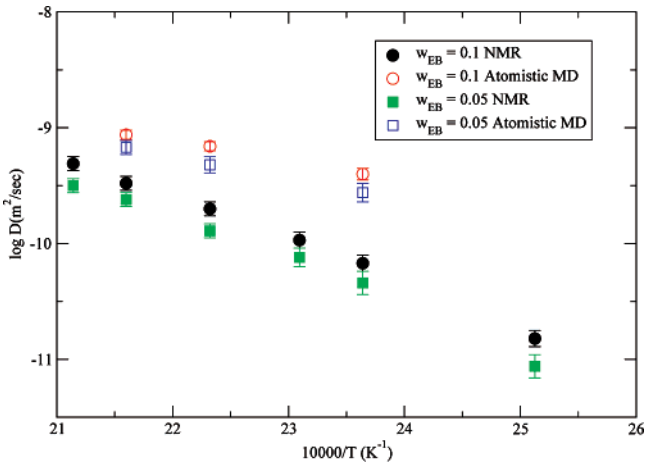

Figure 7. Diffusion coefficient of EB from PFG NMR experiments and atomistic simulations.

part of each curve one can obtain the self-diffusion of coefficient of EB, D_{EB}.

Figure 7 and Table 3 summarize these findings from the UA atomistic *NPT* MD simulations in comparison to the NMR experiments. In Figure 7 D_{EB} is plotted vs the inverse temperature for two EB concentrations, $w_{EB} = 0.1$ (10%) and $w_{EB} = 0.05$ (5%) respectively. Because of the small size of the atomistic systems data for the lower concentrations of EB, $w_{EB} = 0.01$, could not reliably obtained by atomistic simulations. As expected the diffusion constant D_{EB} decreases with the decrease of

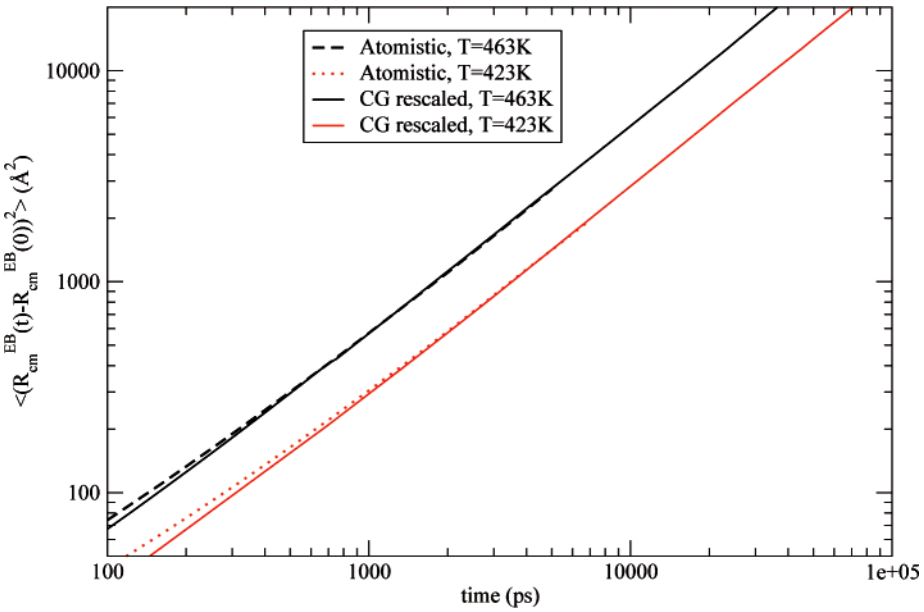

Figure 8. Time mapping of the mesoscopic dynamic simulations using atomistic data for two PS/EB mixture ($w_{EB} = 0.1$, $T = 463$ K and $w_{EB} = 0.1$, $T = 423$ K).

temperature and increases for higher EB concentration. This is displayed by both experiment and simulation. So far the atomistic MD simulations describe the dependence of D_{EB} on temperature and concentration of EB qualitatively correct. However there is a clear quantitative difference to the experimental results. Diffusion coefficients obtained from atomistic simulations are larger than their experimental counterparts by a factor ranging from 3 (for $w_{EB} = 0.1$, $T = 463$ K) to 7 (for $w_{EB} = 0.1$, $T = 423$ K). This is not really surprising and related to the fact that a united-atom model is used in the present work. As it has been also found in the literature UA models overestimate the diffusion of small molecules in a polymer matrix[45] and the reported activation barriers for penetrant motion are smaller with UA models[46] compared to an all atom description. Qualitatively this can be explained by the fact that the inclusion of hydrogens in carbons yielding spherical symmetric CH_x potentials results in a reduced local friction, and thus higher mobility (diffusion). Since also some corrugation of the (all-atom, AA) potential energy landscape has disappeared the activation energy barriers for the motion of the molecules become smaller causing a weaker temperature dependence. Therefore, significant differences for the diffusion of small penetrants in a polymer matrix can be found depending on whether a UA or an AA model is used. It should be noted that the nonbonded interactions in the TraPPE UA model used here, are obtained from phase equilibria MC simulations,[35] and are not optimized to reproduce any short time dynamical quantity of PS. Taking this into account, the qualitative agreement to experiment is surprisingly good.

4.2.2. Dynamics of EB: CG vs Atomistic (UA) Simulations. One of the main goals of the present work is to examine the ability of CG mesoscopic simulations to predict dynamical properties of polymer−penetrant mixtures. Despite the large number of CG models in the literature, the possibility to quantitatively describe the dynamics of polymer−penetrant systems at the CG level, according to our knowledge, has not been investigated up to now. Because of that and in order to better understand different sources of deviations or agreement, we compare the CG results first to the atomistic simulations.

The high efficiency of the CG models occurs upon the reduction in the number of degrees of freedom. This eliminates strongly fluctuating forces corresponding to atomistic degrees of freedom, which eventually produce the large molecular friction. As mentioned before, to a certain extent this holds already for the applied united atom model. CG simulations have an intrinsic time unit τ defined by the parameters of the model. Even though the unit of τ is that of a time, this is not necessarily the physical time scale. To employ CG simulations for a quantitative analysis of time dependent phenomena we have to determine the scaling factor and to check the minimal length scale down to which this applies.[50] In the context of mean-square displacements of polymer beads and additives it is more convenient to argue in terms of bead and particle friction, as this directly enters as a prefactor in the different universal power laws for the motion.[32,43] The friction in the CG description is smaller than the one predicted by the more detailed microscopic force field, i.e., $\zeta_{CG} < \zeta_{AT}$. This leads to the most direct way to identify time scales by mapping the mean-square displacements of the CG simulations onto the data from the atomistic simulations. Because the length scales are fixed by the CG procedure itself from the very beginning, only a time shift factor is available to fit the displacement curves. Figure 8 shows the time mapping for two specific systems, i.e., $w_{EB} = 0.1$, $T = 463$ K and $w_{EB} = 0.1$, $T = 423$ K. Dashed and dotted lines represent the MSDs obtained directly from the atomistic MD simulations. Full lines denote the CG MSDs rescaled in order to match the atomistic data in the linear regime. Diffusion coefficients taken from the CG simulations, D_{EB}^{CG}, before the time mapping (in units of $Å^2/\tau$), as well as the rescaled ones (in units of $Å^2$/ps) are shown in Table 3. The scaling factor, τ_x, in order to bring the CG curves on top of the atomistic, is 7.37 and 13.125 τ/ps at $T = 463$ K and $T = 423$ K, respectively.[51] Both curves in Figure 8 follow, as expected, exactly each other for distances above around 10−14 Å (100−200 $Å^2$) and for times above a few hundreds of ps. This length scale is similar to the one found from the local packing description (see Figure 4), i.e., deviations in the intermolecular $g(r)$ curves for the EB−PS and the PS−PS correlations from the CG simulations match the atomistic curves after a distance of about 10−14 Å. It should be noted that the same length scale is observed if one compares the segmental polymer MSDs in the CG and the atomistic

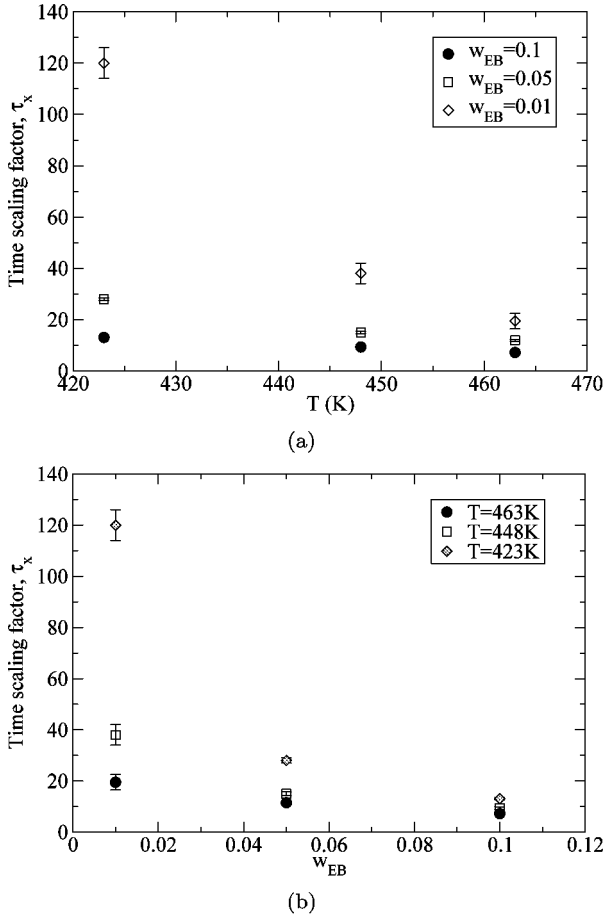

Figure 9. Time mapping factor for different systems: (a) as a function of temperature; (b) as a function of EB concentration.

description.[44] For the calibration of the CG dynamics only relatively short atomistic runs of up to about 1000 ps are sufficient, since only the proper overlap of the curves is required. Comparing this to Figure 6 shows, that at least an order of magnitude more is needed to determine D_{EB} directly from the atomistic simulations. The time scaling factor τ_x (since the friction coefficient is inversely proportional to diffusivity, $\tau_x = \zeta_{AT}/\zeta_{CG}$) for all the systems studied in this work is shown in Figure 9, parts a and b. As we can see (Figure 9a) τ_x decreases as temperature increases; i.e. increase of temperature causes a more rapid increase of D_{EB}^{AT} as compared to D_{EB}^{CG}. The effect of penetrant concentration (Figure 9b) is analogous to that of the temperature: an increase of penetrant concentration leads to a decrease of the time scaling factor. Thus, the relative softening of the landscape in the mesoscopic description is less strong for the systems with larger concentration of EB, leading to smaller τ_x values.

4.2.3. Time Scaling and Relation to Experiment. So far the results do not reveal a clear answer as to what extent CG simulations can be used to study the diffusion of additives in a polymeric matrix. The atomistic simulations follow the experimental data, however with a clear shift in the time scaling. In a similar way the CG data follow the atomistic results with an EB concentration and temperature-dependent time scaling factor τ_x. On the other hand, it is known that coarse grained simulations for polymer dynamics can rather well reproduce the characteristic Vogel−Fulcher behavior of diffusivity and bead friction exhibited by glass forming polymers,[13,47] because polymer dynamics is mostly governed by intermolecular effects on the scale of the polymer polymer strand distance and beyond. This includes the formation and destruction of larger cavities, because

Table 4. Constants of the Arrhenius Type of Dependence of τ_x (see Eq 2) Obtained Using Data from Two Temperatures (T = 448 K and T = 463 K)

w_{EB}	A/k_B (K)	c (τ/ps)
0.1	2850 ± 100	0.012 ± 0.005
0.05	4500 ± 150	0.0006 ± 0.00012
0.01	7050 ± 300	0.000007 ± 0.000002

of the chain connectivity. Thus, the mobility of the additive on mesoscopic and large scales is intimately linked to the structural relaxation of the polymer melt. This relates to time scales much larger than those of the local spacial fluctuation of EB in the rather rugged cavities.[24] Thus, we assume that the motion of EB in presence of the polymeric matrix can be described by two, connected contributions, where the local motion is described by an Arrhenius type mechanism in a temperature and concentration dependent very slowly varying environment. Assuming that the slow component is well captured by the CG polymer model, we describe the dependence of $\tau_x(T)$ on temperature in an empirical way through the Arrhenius equation:

$$\tau_x = c \exp(A/kT) \qquad (2)$$

c is a constant, dependent on the solvent concentration, and A is an "activation energy" quantifying the extent by which activation barriers for penetrant motion in the CG system are reduced relative to the atomistic system. Since $\tau_x(T) = \zeta_{AT}/\zeta_{CG}$, the non-Arrhenius character of ζ_{AT} also holds in the same way for ζ_{CG}. Thus, the procedure does not require the assumption that penetrant diffusion follows an Arrhenius temperature dependence. In other words, the coarse grained model properly takes into account those structural aspects, which are responsible for the non-Arrhenius behavior of the dynamics of the polymeric material. Assuming a relation of the form of eq 2 and using the data from the time mapping, the constants A and c can be calculated. The values of these constants, obtained from the data for τ_x at the two higher temperatures (T = 448 K and T = 463 K), are reported in Table 4. On the basis of these values of A and c, τ_x was computed at the lower temperatures, including T = 398 K, where atomistic simulation are no longer available.

Diffusivities D_{EB} of EB obtained from CG simulations (empty symbols) by the above procedure and PFG NMR experiments (full symbols) for all the systems studied in this work, are shown in Figure 10 as a function of inverse temperature. Note that the temperature dependence of the experimental and simulation data is non-Arrhenius. Diffusion coefficients from the CG simulations for the w_{EB} = 0.1 and w_{EB} = 0.05 systems at the two higher

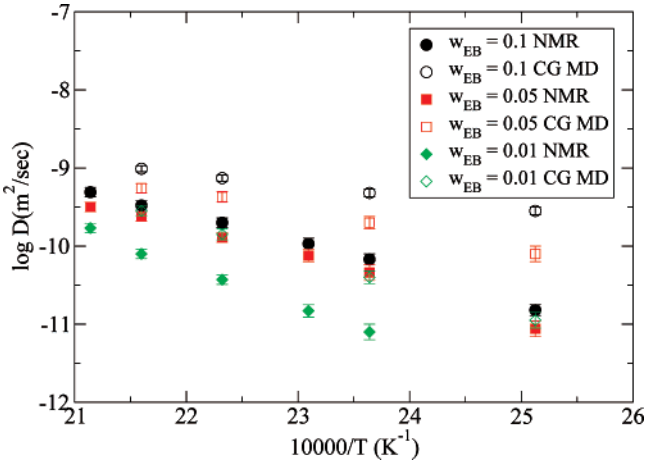

Figure 10. Diffusion coefficient of EB from PFG NMR experiments and coarse-grained simulations as a function of temperature.

temperatures ($T = 448$ K and $T = 463$ K) match, within the error bars, the atomistic simulations. However, additional data for $w_{EB} = 0.01$ systems and for lower temperatures ($T = 398$ K, 423 K) for all w_{EB} systems are presented.[52] The CG results display the same semiquantitative agreement with experimental data as the data for the other systems. However the central advantage is that these points have been obtained exclusively from very fast CG dynamic simulations!

This suggests that using atomistic data for a few reference systems and an Arrhenius-type relation (eq 2) for the time mapping, fast CG simulations can be used to quantitatively predict the dynamics of polymer/penetrant systems in a range of temperatures or/and concentrations, which are not accessible by atomistic simulations to a reasonable accuracy. Finally, the agreement with the experimental data probably can be further improved if an all-atom model is used in the atomistic simulations.

5. Conclusions

In the present work a combined simulation-experimental study of the structure and the dynamics of a polymer/penetrant system has been presented. As a test case the method has been applied to atactic polystyrene(PS)/ethylbenzene(EB) mixtures. The structure of PS/EB systems is analyzed at the level of the intermolecular pair distribution function $g(r)$. For the dynamics of the PS/EB systems, the EB self-diffusion coefficient, D_{EB}, was calculated from atomistic MD simulations. Additionally, on the same systems, PFG NMR experiments have been performed and the simulation predictions have been compared against the experimental self-diffusion data. The MD simulations were found to describe semiquantitatively the experimental results. The differences between the atomistic simulation data and the experimental values are due to the use of a united-atom description in the atomistic runs. This has been also found in the literature and leads to an overestimate the diffusion of small molecules in a polymer matrix. Because of the increase of computer power, the necessary atomistic runs in the future will be performed by all atom simulations.

The main goal of the present work has been to examine the ability of coarse-grained simulations to predict quantitatively the dynamics of the penetrant in polymer/penetrant mixtures. The smaller number of degrees of freedom of the CG model compared to the atomistic (real) model prevents the direct application of the CG model for a quantitative description of the penetrant dynamics in a polymer/penetrant system. To overcome this, we have presented a modeling approach that combines fast CG MD simulations and atomistic MD simulations at high temperatures (reference temperatures) allowing for a mapping of the time unit in the CG description. The time scaling factor, τ_x, used to equate the ethylbenzene MSDs from the CG runs to the data obtained from the atomistic runs was calculated at two reference temperatures. Assuming that the motion of EB relative to the polymer can be viewed (to a first approximation) as a standard Arrhenius-like process embedded in a temperature-dependent slowly varying environment, where the latter is well captured by the coarse grained model, we derive an estimate for the scaling factor τ_x in a broad range of temperatures. This allows us to extend the range of temperatures and penetrant concentrations that can be simulated far beyond what is feasible with atomistic simulations. The most severe shortcoming in this context was the use of a united atom model for the atomistic calibration. On the other hand, this proves that even with moderate effort semiquantitative results can be obtained. Future work will certainly employ all atom models on the atomistic side. There we expect a truly quantitative agreement to experiments. Another interesting aspect, which should help to lead to a better general understanding of coarse graining procedures will be the study of time mapping as a function of the molecular size of the penetrant.

Acknowledgment. We are grateful to W. Loth, K. Knoll, B. Hess, T. Vettorel, and V. Marcon for stimulating discussions.

References and Notes

(1) *Diffusion in Polymers*; Neogi, P., Ed.; University of Missouri—Rolla: Rolla, MO, 1996.
(2) *Monte Carlo and Molecular Dynamics Simulations in Polymer Science*; Binder, K., Ed.; Oxford University Press: New York, 1995.
(3) J. Baschnagel, K. Binder, P. Doruker, A. A. Gusev, O. Hahn, K. Kremer, W. L. Mattice, F. Müller-Plathe, M. Murat, W. Paul, S. Santos, U. W. Suter, V. Tries. Bridging the Gap Between Atomistic and Coarse-Grained Models of Polymers: Status and Perspectives. In *Advances in Polymer Science: Viscoelasticity, Atomistic Models, Statistical Chemistry*; Springer-Verlag Berlin, 2000; Vol. 152, p 41.
(4) Kremer, K.; Müller-Plathe, F. *MRS Bull.* **2001**, no. 26, 205.
(5) Harmandaris, V. A.; Mavrantzas, V. G. In *Simulation Methods for Polymers*; Theodorou, D. N.; Kotelyanski, M., Eds.; Marcel Dekker: New York, 2004.
(6) Ertl, H.; Ghai, R. K.; Dullien, F. A. *AIChE J.* **1974**, *20*, 1.
(7) Vrentas, J. S.; Duda, J. L. *J. Polym. Sci.* **1977**, *15*, 403; **1977**, *15*, 417.
(8) Cohen, M. H.; Turnbull, D. *J. Chem. Phys.* **1959**, *31*, 1164.
(9) Bueche, F. *Physical Properties of Polymers*; Interscience: New York, 1962.
(10) Von Meerwall, E.; Feick, E. J.; Jang, J.; Mattice, W. L. *J. Chem. Phys.* **1998**, *108*, 4299.
(11) Von Meerwall, E.; Feick, E. J.; Ozisik, R.; Mattice, W. L. *J. Chem. Phys.* **1999**, *111*, 750.
(12) Waggoner, R. A.; Blum, F. D.; MacElroy, J. M. D. *Macromolecules* **1993**, *26*, 6841.
(13) Ferry, John, D. *Viscoelastic Properties of Polymers*; John Wiley and Sons: New York, 1980.
(14) Takeuchi, H.; Okazaki, K. *J. Chem. Phys.* **1990**, *92*, 5643.
(15) Takeuchi, H. *J. Chem. Phys.* **1990**, *93*, 2062.
(16) Takeuchi, H.; Okazaki, K. *J. Chem. Phys.* **1990**, *93*, 9042.
(17) Müller-Plathe, F. *J. Chem. Phys.* **1991**, *94*, 3192.
(18) Müller-Plathe, F.; Rogers, S. C.; Van Gunsteren, W. F. *Chem. Phys. Lett.* **1992**, *199*, 237.
(19) Sok, R. M.; Berendsen, H. J. C.; Van Gunsteren, W. F. *J. Chem. Phys.* **1992**, *96*, 4699.
(20) Gusev, A. A.; Suter, U. W. *J. Chem. Phys.* **1993**, *99*, 2228.
(21) Van der Vegt, N. F. A.; Briels, W. J.; Wessling, M.; Strathmann, H. *J. Chem. Phys.* **1996**, *105*, 8849.
(22) Chassapis, C. S.; Petrou, J. K.; Petropoulos, J. H.; et. al. *Macromolecules* **1996**, *29*, 3615.
(23) Van der Vegt, N. F. A.; Briels, W. J.; Wessling, M.; Strathmann, H. *J. Chem. Phys.* **1998**, *108*, 9558.
(24) Hahn, O.; Mooney, D. A.; Müller-Plathe, F.; Kremer, K. *J. Chem. Phys.* **1999**, *111*, 6061.
(25) Harmandaris, V. A.; Angelopoulou, D.; Mavrantzas, V. G.; Theodorou, D. N. *J. Chem. Phys.* **2002**, *116*, 7656.
(26) Harmandaris, V. A.; Doxastakis, M.; Mavrantzas, V. G.; Theodorou, D. N. *J. Chem. Phys.* **2002**, *116*, 436.
(27) Heuchel, M.; Hofmann, D.; Pullumbi, P. *Macromolecules* **2004**, *37*, 201.
(28) Neyertz, S.; Brown, D. *Macromolecules* **2004**, *37*, 10109.
(29) Padding, J. T.; Briels, W. J. *J. Chem. Phys.* **2002**, *117*, 925.
(30) Leon, S.; Delle Site, L.; Van der Vegt, N. F. A.; Kremer, K. *Macromolecules* **2005**, *38*, 8078.
(31) Hess, B.; Leon, S.; Van der Vegt, N. F. A.; Kremer, K. *Soft Matter* **2006**, *2*, 409.
(32) Kremer, K. In *Proceedings of the International School of Solid State Physics-34th Course: Computer Simulations in Condensed Matter: from Materials to Chemical Biology*; Binder, K., Ciccoti, G., Eds.; Erice: 2006.
(33) Sun, Q.; Faller, R. *Macromolecules* **2006**, *39*, 812.
(34) Harmandaris, V. A.; Adhikari, N. P.; Van, der Vegt, N. F. A.; Kremer, K. *Macromolecules* **2006**, *39*, 6708.
(35) Wick, C. D.; Martin, M. G.; Siepmann, J. I. *J. Phys. Chem. B* **2000**, *104*, 8008.
(36) Kremer, K.; Grest, G. *J. Chem. Phys.* **1990**, *92*, 5057.
(37) Berendsen, H. J. C.; Van der Spoel, D.; Van Drunen, R. *Comput. Phys. Commun.* **1995**, *91*, 43.

(38) Berendsen, H. J. C.; Postma, J. P. M.; Di Nola, A.; Haak, J. R. *J. Chem. Phys.* **1984**, *81*, 3684.
(39) Mark, J.; Ngai, K.; Graessley, W.; Mandelkern, L.; Samulski, E.; Koenig, J.; Wignall, G. *Physical Properties of Polymers*, 3rd ed; Cambridge University Press: Cambridge, U.K., 2003.
(40) Soddemann, T.; Dünweg, B.; Kremer, K. *Phys. Rev. E* **2003**, *68*, 046702.
(41) Dünweg, B. *J. Chem. Phys.* **1993**, *99*, 6977.
(42) http://www.espresso.mpg.de/. Arnold, A.; Mann, B.A.; Limbach, H. J.; Holm, C. *Comput. Phys. Commun.* **2006**, *174*, 704.
(43) Doi, M.; Edwards, S. F. *The Theory of Polymer Dynamics*; Claredon Press: Oxford, England, 1986.
(44) Harmandaris, V. A.; Reith, D.; Van der Vegt, N. F. A.; Kremer, K. DOI:10.1002/macp.200700245.
(45) Müller-Plathe, F.; Rogers, S. C.; Van Gunsteren, W. *Macromolecules* **1992**, *25*, 6722.
(46) Van der Vegt, N. F. A. *Macromolecules* **2000**, *33*, 3153.
(47) Tschöp, W.; Kremer, K.; Batoulis, J.; Buerger, T.; Hahn, O. *Acta Polym.* **1998**, *49*, 75.
(48) Vettorel, T.; Meyer, H. *J. Chem. Theory Comput.* **2006**, *2*, 616.
(49) An alternative way of constructing well-equilibrated atomistic configurations is by back-mapping of the CG ones. This method has been already tested for the PS melts.[34] However the present atomistic simulations have been performed, while the other approach was developed.
(50) Since the motion characteristics for the polymers is determined by both the local friction and the longer range interchain packing, the time scaling for the chains and the additives is eventually different.
(51) Note that for a pure PS atactic melt of 1 kDa at $T = 463$ K, $\tau_x = 12.0$ (τ/ps).[34] A detailed study of the dependence of τ_x on the length (M_w) of the penetrant will be part of a following work.
(52) For $w_{EB} = 0.01$ the atomistic data allow for a reasonably accurate time mapping and determination of A and c, because for this one does not need the long time, large distance diffusional motion but instead requires precise data on the local rattling in the molecular surroundings.

MA070201O